Gamow-shell-model description of Li isotopes and their mirror partners

X. Mao (毛兴泽),[1,2] J. Rotureau,[1] W. Nazarewicz,[3,2] N. Michel,[4] R. M. Id Betan,[5,6] and Y. Jaganathen[7]

[1]*National Superconducting Cyclotron Laboratory, Michigan State University, East Lansing, Michigan 48824, USA*
[2]*Department of Physics and Astronomy, Michigan State University, East Lansing, Michigan 48824, USA*
[3]*Facility for Rare Isotope Beams, Michigan State University, East Lansing, Michigan 48824, USA*
[4]*Institute of Modern Physics, Chinese Academy of Sciences, Lanzhou, Gansu 730000, China*
[5]*Physics Institute of Rosario (CONICET), Rosario, Argentina*
[6]*Department of Physics FCEIA (UNR), Rosario, Argentina*
[7]*Institute of Nuclear Physics, Polish Academy of Sciences, PL-31342 Kraków, Poland*

(Received 6 April 2020; revised 15 June 2020; accepted 15 July 2020; published 7 August 2020)

Background: Weakly bound and unbound nuclei close to particle drip lines are laboratories of new nuclear structure physics at the extremes of neutron/proton excess. The comprehensive description of these systems requires an open quantum system framework that is capable of treating resonant and nonresonant many-body states on equal footing.
Purpose: In this work, we develop the complex-energy configuration interaction approach to describe binding energies and spectra of selected $5 \leqslant A \leqslant 11$ nuclei.
Method: We employ the complex-energy Gamow shell model (GSM) assuming a rigid ^{4}He core. The effective Hamiltonian, consisting of a core-nucleon Woods-Saxon potential and a simplified version of the Furutani-Horiuchi-Tamagaki interaction with the mass-dependent scaling, is optimized in the *sp* space. To diagonalize the Hamiltonian matrix, we employ the Davidson method and the Density Matrix Renormalization Group technique.
Results: Our optimized GSM Hamiltonian offers a good reproduction of binding energies and spectra with the root-mean-square (rms) deviation from experiment of 160 keV. Since the model performs well when used to predict known excitations that have not been included in the fit, it can serve as a reliable tool to describe poorly known states. A case in point is our prediction for the pair of unbound mirror nuclei ^{10}Li - ^{10}N in which a huge Thomas-Ehrman shift dramatically alters the pattern of low-energy excitations.
Conclusion: The new model will enable comprehensive studies of structure and reactions aspects of light drip-line nuclei.

DOI: 10.1103/PhysRevC.102.024309

I. INTRODUCTION

With progress in radioactive beam experimentation and many impressive advances in microscopic nuclear theory, light nuclei provide an excellent ground for testing both nuclear interactions and many-body approaches. Of particular interest are weakly bound and unbound nuclear systems with extreme neutron-to-proton imbalance, whose structure is profoundly affected by the coupling to the continuum of decay and reaction channels [1–4].

The important challenge for the field of low-energy nuclear theory is to unify nuclear bound states with resonances and scattering continuum within one consistent framework [5]. There are many open questions that can be answered by studying drip-line systems [6]: What can be said about properties of weakly bound or unbound many-body systems close to the reaction threshold? Do their properties depend on any particular realization of the Hamiltonian? Which nuclear properties are impacted by the coupling to the continuum of scattering and decaying states? Theoretically, a coherent description of the interplay between bound and unbound states in the many-body system requires an open quantum system formulation. In this context, this area of research is truly interdisciplinary. Indeed, open quantum systems are studied in various fields of physics: nuclear physics, atomic and molecular physics, nanoscience, quantum optics, etc. In spite of their differences, such systems often display universal properties that are common to all weakly bound or unbound systems close to the reaction/decay threshold.

Impressive progress has been achieved in describing weakly bound and unbound nuclei using *A*-body methods rooted in realistic inter-nucleon interactions [7–11]. Examples include microscopic computations of ^{11}Be [12,13], ^{7}He [14–16], and ^{9}He [17].

On a more phenomenological level, configuration integration techniques, based on the concept of valence nucleons coupled to an inert core have reached a high level of sophistication. Approaches such as the real-energy continuum shell model [18,19] and shell model embedded in the continuum [20–23] have been applied to systems near particle-emission threshold with one/two nucleons allowed in the continuum space. Another powerful tool is the complex-energy Gamow shell model (GSM) [24–26], an extension of the interacting shell model to the treatment of open quantum systems. GSM has been successfully used to describe structural and reaction

properties of exotic nuclei (see Refs. [27–31] for recent representative applications).

This study can be viewed as a continuation of previous work on the development of a quantitative GSM description of light nuclei using a ^{4}He-nucleon potential and finite-range interaction between valence nucleons. In the first paper [31], where calculations were carried out in the *spdf* model space, the core-nucleon potential was optimized to nucleon-^{4}He phase shifts. By means of the principal-component analysis, it was concluded that a very reasonable description of energies of $6 \leqslant A \leqslant 9$ nuclei (with the root-mean-square (rms) deviation from experiment of 250 keV) could be achieved with only four interaction parameters. In the follow-up study [32], where calculations were performed in the *spd* space, experimental energies and widths of $^{5-8}$He could be reproduced within tens of keV precision by adjusting only one parameter (the strength of spin-singlet central neutron-neutron term). In this work, we use the GSM model to describe binding energies and spectra of $5 \leqslant A \leqslant 11$ nuclei in the *sp* space by carrying out simultaneous optimization of the core-nucleon potential and the valence two-body interaction with the mass-dependent interaction scaling to effectively account for the missing three-body forces. We show that with the appreciable reduction of the parameter space (four strengths of the core-nucleon potential and four parameters of the two-body interaction), a very reasonable agreement with experimental energies is obtained.

Predictions were also made for the particle-unstable nuclei ^{10}Li, ^{10}N, and ^{11}O, which are excellent laboratories of open quantum system physics. In particular, a spectacularly strong Thomas-Ehrman effect in the ^{10}N - ^{10}Li mirror pair is predicted.

This paper is organized as follows. The theoretical model is outlined in Sec. II, which contains a short overview of GSM, description of the GSM Hamiltonian, and the optimization protocol. Results are presented in Sec. III, with the optimization results discussed first, followed by predictions for lithium isotopes and their mirror partners. Finally, Sec. IV presents conclusions and perspectives for future studies.

II. THEORETICAL MODEL

A. Gamow shell model

Here we briefly recall the GSM formalism. In this work, we describe the lithium isotopes and their mirror partners in terms of valence nucleons coupled to the ^{4}He core. This picture is justified by the fact that the ^{4}He nucleus is a tightly bound system with the first excited state located 20.21 MeV above the ground state (g.s.) [33].

The GSM Hamiltonian can be written as

$$H = \sum_{i}^{N_{\rm val}} \left[\frac{\boldsymbol{p}_i^2}{2\mu_i} + U_{\rm c}(i) \right] + \sum_{i=1, j>i}^{N_{\rm val}} \left[V_{i,j} + \frac{\boldsymbol{p}_i \boldsymbol{p}_j}{M_{\rm c}} \right], \quad (1)$$

where $N_{\rm val}$ denotes the number of valence nucleons, μ_i and $M_{\rm c}$ are the reduced mass of the nucleon and the mass of the core, respectively, $U_{\rm c}$ is the core-nucleon potential, and $V_{i,j}$ is the interaction between valence nucleons. The Hamiltonian Eq. (1) is written in the cluster-orbital shell model coordinates [34] defined with respect to the center of mass of the core.

The GSM Hamiltonian is diagonalized in the Berggren basis [35], which allows to consistently treat bound, resonance, and scattering states. In the complex-momentum space, the Berggren basis obeys the closure relation for each partial wave (ℓ, j):

$$\sum_{n=b,d} |\tilde{u}_n\rangle \langle u_n| + \int_{\mathcal{L}^+} |\tilde{u}(k)\rangle \langle u(k)| \, dk = 1, \quad (2)$$

where b and d stand for the bound states and selected decaying resonant states, respectively, and the contour $\mathcal{L}^+$ representing the nonresonant scattering states is located in the fourth quadrant of the complex k-plane. The specific shape of $\mathcal{L}^+$ is not important as long as all resonant states between the real axis and the contour $\mathcal{L}^+$ are included. In practical applications, the contour is discretized for each (ℓ, j), which results in a finite number of single-particle (s.p.) states. From this discretized set of shells one constructs Slater determinants, which form a many-body basis within which the GSM Hamiltonian is diagonalized. Due to the inclusion of resonances and complex-momentum scattering states, the Hamiltonian representation in the Berggren basis is complex symmetric [26].

As in any configuration interaction approach, the dimension of the Hamiltonian matrix grows quickly with the number of active particles. In the context of the GSM, it increases more quickly than in the conventional shell model due to the presence of discretized scattering states. To this end, we truncate the model space by working with natural orbitals which provide an optimized set of s.p. states [31,36,37].

The natural orbitals are first computed in a truncated space where few valence particles are allowed to occupy continuum shells. A truncation is then performed on the s.p. basis by keeping only natural orbitals for which the modulus of the occupation number is greater than a certain (small) value. Finally, a new set of Slater determinants is constructed, for which also a truncation on the number of particles in the continuum is enforced, and the numerical diagonalization is performed using the Davidson method [38].

To check the accuracy of this truncation procedure in the case of the largest systems, a supplementary computation was also performed using the density-matrix renormalization group (DMRG) [39,40] method. The DMRG allows performing calculations without the s.p. particle basis truncation and without restrictions on the number of particles in the continuum. In this approach, the many-body Schrödinger equation is solved iteratively in tractable truncated spaces, which are gradually increased until the numerical convergence is reached. We have checked that, in all cases discussed in this work, the GSM results are in good agreement with those of DMRG (see more discussion in Sec. II D).

B. GSM Hamiltonian

The core-nucleon potential is taken as a Woods-Saxon (WS) field, with a central and spin-orbit terms, and the Coulomb field for protons:

$$U_{\rm c}(r) = V_0 f(r) - 4V_{\ell s} \frac{1}{r} \frac{df(r)}{dr} \boldsymbol{\ell} \cdot \boldsymbol{s} + U_{\rm Coul}(r), \quad (3)$$

where $f(r) = -(1 + \exp[(r - R_0)/a])^{-1}$. The WS radius R_0 and diffuseness a were taken from Ref. [31]: $R_0(n) = 2.15$ fm, $R_0(p) = 2.06$ fm, $a(n) = 0.63$ fm, and $a(p) = 0.64$ fm. The Coulomb potential is generated by a spherical Gaussian charge distribution with radius $R_{\rm ch} = 1.681$ fm [41].

Following Ref. [31], the interaction between valence nucleons is a sum of central, spin-orbit, tensor, and Coulomb terms:

$$V = V_c + V_{LS} + V_T + V_{\rm Coul}. \tag{4}$$

The central, spin-orbit and tensor interactions are constructed based on the finite-range Furutani-Horiuchi-Tamagaki (FHT) force [31,42,43]. For each term, the radial form factor is represented by a sum of three Gaussians with different widths representing the short, intermediate, and long ranges of the nucleon-nucleon interaction. This interaction has been used successfully to describe structure and reactions involving light nuclei [28–32,44,45].

To be applied in the present GSM formalism, the interaction is rewritten in terms of the spin-isospin projectors Π_{ST} [46]:

$$\begin{aligned} V_{\rm c}(r) &= V_c^{11} f_c^{11}(r)\Pi_{11} + V_c^{10} f_c^{10}(r)\Pi_{10} \\ &\quad + V_c^{00} f_c^{00}(r)\Pi_{00} + V_c^{01} f_c^{01}(r)\Pi_{01}, \\ V_{\rm LS} &= (\boldsymbol{L}\cdot\boldsymbol{S})\, V_{LS}^{11} f_{LS}^{11}(r)\Pi_{11}, \\ V_{\rm T}(r) &= S_{ij}\big[V_T^{11} f_T^{11}(r)\Pi_{11} + V_T^{10} f_T^{10}(r)\Pi_{10}\big], \end{aligned} \tag{5}$$

where $r \equiv r_{ij}$ stands for the distance between the nucleons i and j, $\hat{r} = \boldsymbol{r}_{ij}/r_{ij}$, $\boldsymbol{L}$ is the relative orbital angular momentum, $\boldsymbol{S} = (\boldsymbol{\sigma}_i + \boldsymbol{\sigma}_j)/2$, and $S_{ij} = 3(\boldsymbol{\sigma}_i \cdot \hat{r})(\boldsymbol{\sigma}_j \cdot \hat{r}) - \boldsymbol{\sigma}_i \cdot \boldsymbol{\sigma}_j$. The interaction Eq. (5) is characterized by the seven interaction strengths in spin-isospin channels, V_c^{11}, V_c^{10}, V_c^{00}, V_c^{01}, V_{LS}^{11}, V_T^{11}, and V_T^{10}.

In Ref. [31], the FHT interaction was used in the GSM description of bound and unbound nuclei with $A \leqslant 9$. While a good energy reproduction was achieved, the systematic statistical study of the parameters carried out in Ref. [31] demonstrated that some of the terms in the FHT interaction were sloppy, i.e., not well constrained.

In this study, we use a simplified version of the FHT interaction where we consider the central V_c^{10}, V_c^{01}, and tensor V_T^{10} terms. This choice is not only informed by the previous statistical work [31] but also justified by effective field theory (EFT) arguments [47–51]. Indeed, in the EFT expansion of the bare nucleon-nucleon interaction, these three terms appear at leading order, whereas the other terms present in the original FHT interaction correspond to higher orders of EFT. However, we have observed that adding the central term V_c^{00} improves the overall description of the nuclei considered in this work and hence we have also included it in $V_{i,j}$. We want to mention here that a similar approach was employed in Ref. [32] to construct an effective neutron-neutron interaction for the description of the helium isotopic chain in the Berggren basis. In that case, using only the central term V_c^{01}, a good reproduction of weakly bound and unbound states in helium nuclei was achieved.

As it is customary in shell-model studies [52,53], a mass-dependent interaction-scaling factor of the form $(6/A)^\alpha$ is introduced to effectively account for the missing three-body forces [54,55]. We found that the value $\alpha = 1/3$ gives a very reasonable description of experimental energies. Finally, the Coulomb interaction between valence protons is treated by incorporating its long-range part into the basis potential and expanding the short-range two-body component in a truncated basis of HO states [56,57].

C. Interaction optimization protocol

Our interaction optimization protocol strictly follows that of Ref. [31]. In short, we minimize the χ^2 penalty function:

$$\chi^2(\boldsymbol{p}) = \sum_{i=1}^{N_d} \left(\frac{\mathcal{O}_i(\boldsymbol{p}) - \mathcal{O}_i^{\rm exp}}{\delta\mathcal{O}_i} \right)^2, \tag{6}$$

where $\boldsymbol{p}$ is the vector of parameters used, N_d is the number of observables, $\mathcal{O}_i(\boldsymbol{p})$ are the calculated observables, $\mathcal{O}_i^{\rm exp}$ are experimental values, and $\delta\mathcal{O}_i$ are the adopted errors that have been obtained from the χ^2 normalization [58,59].

The minimization of χ^2 is done using the Gauss-Newton method. Since the GSM Hamiltonian is linear in the strength parameters, the Jacobian matrix at the minimum $\boldsymbol{p}_0$,

$$J_{i\alpha} = \frac{1}{\delta\mathcal{O}_i} \frac{\partial\mathcal{O}_i}{\partial p_\alpha}\bigg|_{\boldsymbol{p}_0}, \tag{7}$$

can be calculated exactly using the Hellmann-Feynman theorem [60]. The covariance matrix $\mathcal{C}$ can be expressed in terms of J:

$$\mathcal{C} \simeq (J^T J)^{-1}. \tag{8}$$

In the situation where the Jacobian matrix is noninvertible or has a very small determinant, the Gauss-Newton method becomes unstable. This typically happens when a parameter is sloppy, i.e., not well constrained by observables. To stabilize the calculation, the matrix inversion is replaced by its pseudoinverse, derived from the singular value decomposition (SVD) of the Jacobian matrix [31].

The uncertainties on parameters and predicted observables can be computed with the help of the covariance matrix $\mathcal{C}$. For more details, the reader is referred to Ref. [31].

The four strengths of the WS potential and four parameters of the two-body interaction are simultaneously optimized to reproduce 15 energy levels in lithium isotopes and their mirror partners given in Table I.

The calculations are performed in a model space which includes $s_{1/2}$, $p_{3/2}$, and $p_{1/2}$ partial waves for both protons and neutrons. Since the optimization involves energies only, for the sake of speeding-up the optimization and for better stability, we used a deeper WS potential to generate the basis, in which the $0p_{3/2}$ and $0p_{1/2}$ poles are bound. A real contour was then used to describe the nonresonant continuum space. The contour $\mathcal{L}^+$, independent of interaction parameters, was divided into three segments: $[0, k_{\rm peak}]$, $[k_{\rm peak}, k_{\rm mid}]$, and $[k_{\rm mid}, k_{\rm max}]$, with the values $k_{\rm peak} = 0.25$ fm^{-1}, $k_{\rm mid} = 0.5$ fm^{-1}, and the cutoff momentum $k_{\rm max} = 4$ fm^{-1}. Discretizing each segment with 10 points using the Gauss-Legendre quadrature guarantees the convergence of results.

TABLE I. Energy levels used in the GSM Hamiltonian optimization. The energies are given with respect to the ^{4}He g.s. The experimental values $E_{\rm exp}$ are taken from Ref. [33]. They are compared to the GSM values $E_{\rm GSM}$.

Nucleus	State	$E_{\rm exp}$ (MeV)	$E_{\rm GSM}$ (MeV)
^{6}Li	1^+	−3.70	−3.72
	0^+	−0.14	−0.10
^{7}Li	$3/2^-$	−10.95	−11.02
	$1/2^-$	−10.47	−10.14
^{8}Li	2^+	−12.98	−13.14
	1^+	−12.00	−11.93
^{9}Li	$3/2^-$	−17.05	−16.90
	$1/2^-$	−14.35	−14.50
^{11}Li	$3/2^-$	−17.41	−17.48
^{7}Be	$3/2^-$	−9.30	−9.36
	$1/2^-$	−8.88	−8.53
^{8}B	2^+	−9.44	−9.60
	1^+	−8.67	−8.50
^{9}C	$3/2^-$	−10.74	−10.85
	$1/2^-$	−8.52	−8.59

To calculate resonance's width, one has to generate a basis based on a shallower basis-generating WS potential, in which the $0p_{3/2}$ and $0p_{1/2}$ poles are decaying resonances. In this case, a complex contour defined by a complex value of $k_{\rm peak}$ is employed. It is to be noted that calculation of the width is more demanding than that of energy. A higher discretization with 20 points for each segment was used for this purpose. Due to the Coulomb repulsion, the mean field used to generate the s.p. basis for proton rich nuclei varies with proton number. The contour is adjusted separately for each system to assure that the Berggren completeness relation is met. To ensure the numerical stability, the chosen contour should neither lie too close to the Gamow poles nor lie too far from the real-k axis. In this work, $k_{\rm peak}$ is chosen to lie slightly below the position of the $0p_{3/2}$, $0p_{1/2}$ poles, but with the imaginary part greater than -0.2 fm^{-1}. The calculations were repeated with several slightly different values of $k_{\rm peak}$ to assure the full convergence.

D. Computational details

In this study, we used a newly developed GSM code that is based on the two-dimensional partitioning of the Hamiltonian matrix [61]. First, we computed natural orbitals from a calculation with at most two particles in the continuum space. The s.p. basis was further truncated by keeping the natural orbitals with occupations greater than 10^{-6}. The GSM problem was then solved in a model space with at most four particles in the continuum shells. We checked the accuracy of this truncation by performing full DMRG calculations for the systems with $A = 9$–11.

TABLE II. Central and spin-orbit strengths of the core-nucleon WS potential optimized in this work. The statistical uncertainties are given in parentheses.

Parameter	Neutrons	Protons
V_0 (MeV)	39.5 (2)	42.1 (4)
$V_{\ell s}$ (MeV fm^2)	10.7 (2)	11.1 (5)

The DMRG allows the computations of energies without truncation in the s.p. basis and without restriction on the number of particles in the continuum. In the first stage of the DMRG procedure, the set of shells is split into two subsets H and P: the pole subspace H consists of the Gamow poles considered (for instance, in the DMRG computations of the ^{9}Li g.s., H contains the $0p_{3/2}$ and $0p_{1/2}$ Gamow states) and the remaining shells form the subspace P. The resolution of the Schrödinger equation is then performed in an increasing set of shells, by gradually including the shells of P, one at a time. After having considered a given shell of P, the model space is truncated by keeping $N_{\rm kept}$ many-body states that correspond to the eigenstates of the density matrix with the largest eigenvalues w_i (in modulus). The number of states kept is defined by the control parameter ϵ so that the condition $|1 - \Re(\sum_{i=1}^{N_{\rm kept}} w_i| < \epsilon$ is fullfilled. The first DMRG stage ends when all shells in P have been included. At that point, natural orbitals are computed and new subsets H and P are defined. The new subset H contains N_H natural orbitals. The calculation continues in a similar fashion, by adding shells from the new subset P, one by one, until all shells have been considered, and then a new set of natural orbitals is computed. N_H is increased and ϵ decreased, until convergence (few keV), is achieved. For instance, in the case of the ^{9,11}Li g.s., computations were carried out by increasing N_H up to 12 and ϵ was decreased down to 5×10^{-9} (a typical DMRG accuracy [45]). For both nuclei, the GSM energies turned out to be less than 10 keV above the DMRG results. For more details about our DMRG implementation, see Refs. [37,39,40].

III. RESULTS

A. Optimized interaction

As one can see in Table I, a very good consistency between theoretical and experimental energies has been achieved. The rms deviation from experimental values is 160 keV. The largest discrepancy is obtained for the $1/2^-$ states of ^{7}Li and ^{7}Be, where the deviation from the data is ∼340 keV.

The values of the parameters for the WS potentials and the two-body interaction are displayed, along with their statistical uncertainties, in Tables II and III, respectively. As one can

TABLE III. Strengths V_η^{ST} of the two-body interaction optimized in this work. The statistical uncertainties are given in parentheses.

V_c^{01}(MeV)	−9.425 (70)
V_c^{10}(MeV)	−8.309 (90)
V_c^{00}(MeV)	−8.895 (1130)
V_T^{10}(MeV fm^{-2})	−22.418 (970)

TABLE IV. Ground-state energies (in MeV) and widths (in keV) of ^{5}He and ^{5}Li obtained from the optimized core-nucleon potential and compared to experiment [64,65].

Nucleus	E_{GSM}	E_{exp}	Γ_{GSM}	Γ_{exp}
^{5}He	0.74	0.798	640	648
^{5}Li	1.6	1.69	1300	1230

judge from the small parameter uncertainties in Tables II and III, the GSM Hamiltonian fit is well constrained. As expected [31], the central term V_c^{00} has the largest uncertainty of ∼12%.

It is to be noted that the core-nucleon potential developed in the present study, optimized simultaneously with the two-body interaction, is slightly shallower than the WS field optimized in Ref. [31] to the experimental s and p nucleon-^{4}He scattering phase shifts. To assess the quality of the WS potential obtained in this work, Table IV shows the predicted energies and widths of the $3/2^-$ g.s. of ^{5}He and ^{5}Li. These values are indeed very close to predictions of Ref. [31] for ^{5}He and ^{5}Li.

Figure 1 shows the energies calculated in the GSM for the g.s. and selected excited states in lithium isotopes. Table V lists the energy levels for states not entering the optimization with the corresponding statistical uncertainties. As one can see, the optimized interaction allows for a good reproduction of experimental energies. It is to be noted that the results for higher-excited states not included in the fit are also very satisfactory. For instance, the calculated 3^+ state in ^{6}Li at −1.57 MeV is only 60 keV below the experimental energy. The experimental widths for the second $5/2^-$ state in ^{7}Li (89 keV) and $5/2^-$ state in ^{9}Li (88 keV) are very reasonable: the GSM values are, respectively, 22 keV and 62 keV. In general, we do not expect the same quality of data reproduction for all excited states due to the fact that the higher partial waves with $\ell \geqslant 2$, which may contribute to the wave functions of these states, are not included in the model space. The estimated statistical

TABLE V. Energy levels for states not entering the optimization. The experimental values E_{exp} are taken from Ref. [33]. The GSM values E_{GSM} are shown with the uncertainties in the parenthesis.

Nucleus	State	E_{exp} (MeV)	E_{GSM} (MeV)
^{6}Li	3^+	−1.51	−1.57(2)
^{7}Li	$7/2^-$	−6.3	−6.04(2)
^{8}Li	3^+	−10.73	−10.59(2)
^{9}Li	$5/2^-$	−12.75	−12.64(2)
^{10}Li	2^+	−16.78	−16.55(5)
	1^+	−16.54	−16.22(5)
^{7}Be	$7/2^-$	−4.73	−4.47(2)
^{8}B	3^+	−7.12	−7.11(2)
^{9}C	$5/2^-$	−7.14	−7.12(5)
^{10}N	1^-	−8.84	−8.93(6)
	2^-	−7.94	−8.46(6)

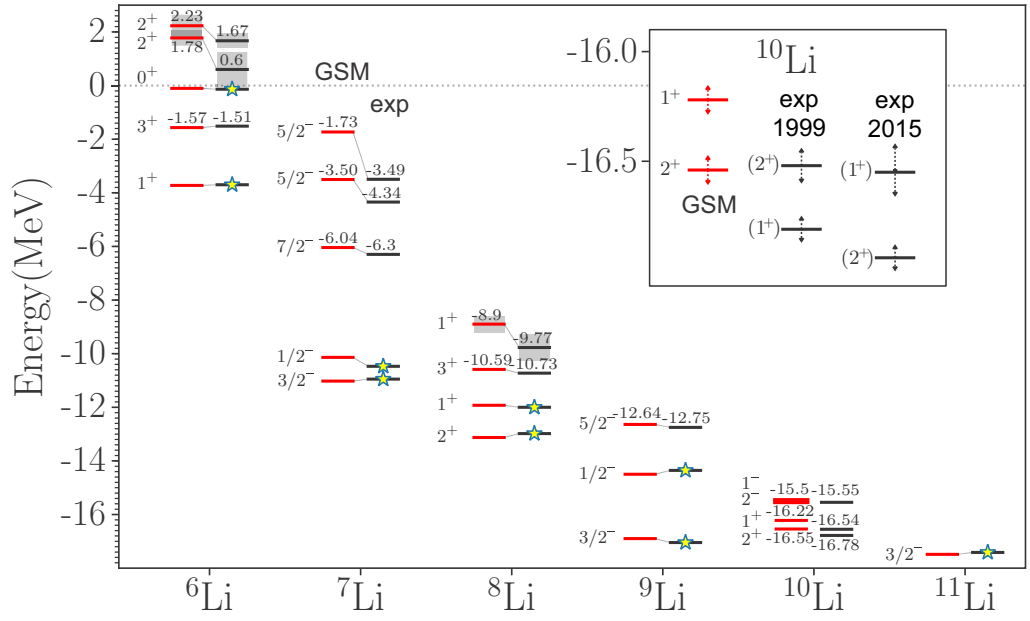

FIG. 1. Level schemes of $^{6-11}$Li calculated in GSM and compared to experiment. Energies are given with respect to ^{4}He core. The resonance widths are marked by shaded boxes. The levels used in the GSM Hamiltonian optimization are marked by stars; their energies are listed in Table I. Theoretical uncertainties for states not entering the optimization are given in Table V. The inset shows the predicted levels of ^{10}Li compared to experimental data from 1999 [62] and 2015 [63]. Uncertainties on these levels are marked by arrows. See text for more discussion.

TABLE VI. Squared amplitudes of dominant configuration of valence neutrons and protons for low-lying levels of ^{10}Li and ^{10}N, respectively. The odd proton in ^{10}Li and the odd neutron in ^{10}N occupy the $0p_{3/2}$ Gamow state. The tilde sign labels nonresonant continuum components.

Configuration	^{10}Li		^{10}N	
	2^+	1^+	2^+	1^+
$(0p_{3/2})^4(0p_{1/2})^1$	0.84	0.81	0.81	0.78
$(0p_{3/2})^3(0p_{1/2})^2$	0.10	0.06	0.10	0.05
	1^-	2^-	1^-	2^-
$(0p_{3/2})^4(1s_{1/2})^1$	0.72	0.73	0.44	0.37
$(0p_{3/2})^4(\widetilde{s_{1/2}})^1$			0.29	0.35
$(0p_{3/2})^3(0p_{1/2})^1(1s_{1/2})^1$	0.14	0.14	0.09	0.07
$(0p_{3/2})^3(0p_{1/2})^1(\widetilde{s_{1/2}})^1$			0.06	0.07
$(0p_{3/2})^2(0p_{1/2})^2(1s_{1/2})^1$	0.07	0.07	0.04	0.03
$(0p_{3/2})^2(0p_{1/2})^2(\widetilde{s_{1/2}})^1$			0.03	0.03

uncertainties on the predicted energies are small: in most cases they are in the range of 20–60 keV.

B. Structure of ^{10}Li

Several experiments [66–69] and theoretical studies [25,70] have indicated that the structure of the g.s. in ^{10}Li may correspond to a valence neutron in a virtual s-state. In a recent experiment [71], the presence of an appreciable low-energy $\ell = 0$ strength has not been confirmed. Their conclusion was, however, challenged in theoretical studies [72,73].

We wish to note, however, that a virtual state in ^{10}Li cannot be associated with an energy level of the system; the appearance of such a state in the complex-momentum plane manifests itself through a low-energy enhancement of the $n + {}^9$Li cross section, see Refs. [25,76,77] for more discussion of this point in the context of the GSM description of ^{10,11}Li. For that reason, we limited our calculations to resonant states in ^{10}Li that can be interpreted as experimentally observable resonances.

The computed g.s. 2^+ and the first excited state 1^+ are predicted, respectively, at 0.35 MeV and 0.68 MeV above the $n + {}^9$Li threshold. As seen in Fig. 1, the practically degenerate 1^- and 2^- states are calculated at 1.05 MeV. A comment is in order here. To achieve the numerical stability, the calculation of the resonances in ^{10}Li had to be performed by employing a basis-generating WS potential that is deeper than the optimized core-nucleon potential. We have checked that in this way we could obtain very stable results for the energies, with accuracy below 1 keV. However, the computed widths, of the order of few hundreds keV, are not stable. For that reason, we do not show them in Fig. 1.

Table VI lists the squared amplitudes of the dominant neutron configurations for the four low-lying states of ^{10}Li. The positive parity states are primarily made from the $0p_{3/2}$ and $0p_{1/2}$ resonant shells. The negative parity states contain one neutron in the $1s_{1/2}$ shell. The contribution from the nonresonant continuum space to the low-lying states is very small.

In Ref. [62] they observed two positive-parity states at 0.24 and 0.53 MeV above the $n + {}^9$Li threshold. The $J^\pi = 1^+$ assignment for the lower state was questioned in Ref. [63] who suggested a $J^\pi = 2^+$ assignment, see the inset in Fig. 1. Considering the large experimental widths of the $1^+/2^+$ doublet, 0.10/0.4 MeV [62] or 0.8/0.2 MeV [63], both experimental results are consistent with the GSM results. The computed position of the negative-parity 1^-, 2^- doublet is consistent with the observation of a negative-parity state at ∼1.5 MeV [71].

C. Mirror partners of lithium isotopes

The level schemes for the mirror partners of lithium isotopes are shown in Fig. 2. As in the Li case, we obtain a very reasonable agreement with experiment. The $5/2^-$ and $7/2^-$ excited states in ^{7}Be are slightly (<300 keV) above the corresponding experimental values, whereas the position of the resonant 3^+ states in ^{8}B and $5/2^-$ state in ^{9}C are well reproduced, as well as the weakly-bound g.s. of ^{8}B and ^{9}C.

In the following we focus on the unbound nuclei ^{10}N and ^{11}O. Due to the presence of the Coulomb barrier, the $1s_{1/2}$ single-proton state is a resonance rather than a virtual state [75,77]. To capture this state, a complex contour is used with a $k_{\rm peak} = (0.25 - 0.05i)$ fm^{-1}.

The spectrum of ^{10}N is not experimentally known with certainty. In Fig. 2, we show the tentative level assignments used in Ref. [33]. According to Refs. [78,79], the g.s. of ^{10}N is most likely a 1^- state of energy in the range from 1.81 to 1.94 MeV. In a more recent work [80], they observed two low-lying negative-parity states but they were not able to assign J^π values.

Our calculations for ^{10}N predict the g.s. to be a 1^- state with $(E, \Gamma) = (-8.93, 0.9)$ MeV that lies 1.92 MeV above the one-proton threshold. The first excited state is predicted to be a 2^- state with $\Gamma = 0.3$ MeV slightly below the value quoted in Ref. [80]. This result is consistent with the recent Gamow coupled-channel analysis of Ref. [77]. We also predict an excited 1^+ state with $\Gamma = 0.3$ MeV, lying 2.9 MeV above the ^{9}C $+p$ threshold, as well as a second positive-parity 2^+ state with a width of 0.36 MeV.

Table VI shows the squared amplitudes of the dominant proton configurations for the four low-lying states of ^{10}N. Similar to ^{10}Li, the positive parity states are primarily made from the $0p_{3/2}$ and $0p_{1/2}$ resonant shells. The dominant configurations of negative parity states contain one $\ell = 0$ proton, which can either be in the $1s_{1/2}$ shell or in a nonresonant continuum state.

The unbound ^{11}O is the mirror partner of the $2n$-halo nucleus ^{11}Li. The first observation of ^{11}O was achieved recently [75]. A broad peak with a width of 3.4 MeV was observed which was interpreted in terms of four overlapping $3/2^-$ and $5/2^+$ resonances. Our GSM calculations predict a $3/2^-_1$ g.s. with a width of 0.13 MeV and the first excited $5/2^+_1$ state with $\Gamma \approx 1$ MeV; see Fig. 2. These predictions are consistent with the Gamow coupled-channel calculations of Ref. [77].

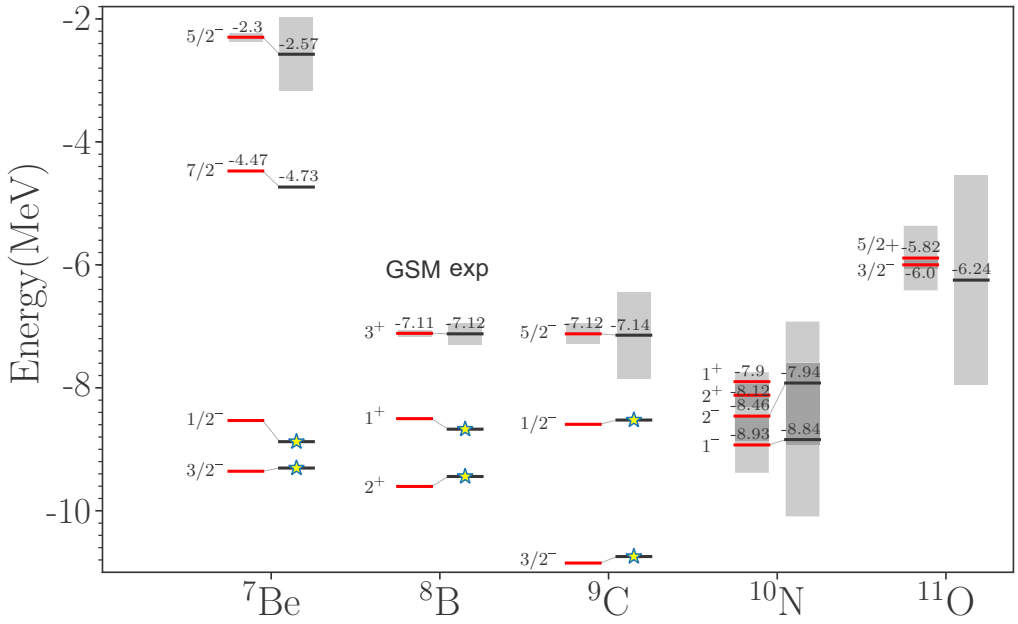

FIG. 2. Similar to Fig. 1 but for the mirror partners of the Li isotopes. Experimental energy of the $5/2^-$ resonance in ^{9}C was taken from Ref. [74] and the data for ^{11}O from Ref. [75].

To study the effect of particle continuum due to different positions of particle thresholds in mirror partners, or Thomas-Ehrman effect [81,82], in Fig. 3 we compare the level schemes of Li isotopes and their mirror partners. (For the early GSM study of the Thomas-Ehrman shifts in light nuclei, see Ref. [28].) As expected, the proton-unbound states in proton-rich mirror nuclei are shifted down in energy as compared to the states in neutron-rich partners, which lie below, or slightly above the one-neutron threshold.

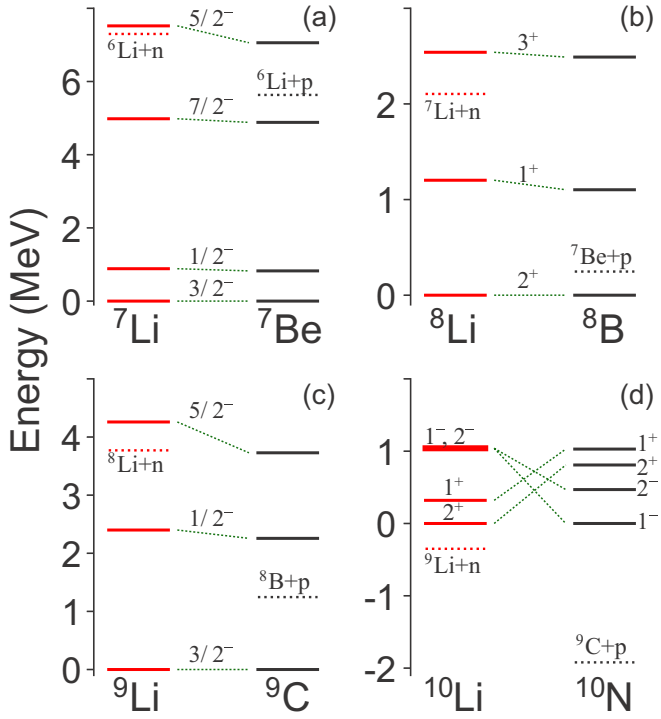

FIG. 3. Level schemes of Li isotopes with (a) $A = 7$, (b) $A = 8$, (c) $A = 9$, (d) $A = 10$, and their mirror partner predicted in our GSM calculations. The energies are plotted with respect to the g.s. energy (at zero). The one-nucleon emission thresholds are marked.

The ^{10}Li - ^{10}N mirror pair is the most interesting one as both nuclei lie above the particle-emission thresholds. As seen in Table VI, the effect of the very low ^{9}C $+p$ threshold in ^{10}N on the negative-parity states 1^- and 2^- containing the s-wave proton is huge: it results in a rather dramatic shift of both negative parity states when going from ^{10}Li to ^{10}N that gives rise to a different structure of low-lying resonances in these nuclei.

IV. CONCLUSIONS

In this work, we studied level schemes of $^{6-11}$Li and their mirror partners in the framework of the complex-energy Gamow shell model assuming the rigid ^{4}He core. The effective interaction between valence nucleons is constructed based on a simplified version of the FHT potential.

By fitting four FHT coupling constants and four parameters of the core-nucleon potential, to the experimental energies of 15 states in $^{6-9,11}$Li, ^{7}Be, ^{8}B, and ^{9}C, we managed to construct a well constrained interaction. A rms deviation from experiment of 160 keV was reached for energy levels used in the GSM Hamiltonian optimization, with the statistical errors of the GSM Hamiltonian parameters not exceeding 12%. This result suggests that the "complex-made-simple" scenario proposed in Ref. [32] for the He chain also works for heavier nuclei involving valence protons. Namely, a parameter reduction guided by effective-scale arguments provides a practical alternative to full-fledged A-body calculations for drip-line nuclei.

We assessed the predictive power of the optimized Hamiltonian by making predictions for excited states not included in the fit. In general, a very reasonable agreement with testing data was obtained; see Table V.

Predictions were also made for the particle-unstable nuclei ^{10}Li, ^{10}N, and ^{11}O. The computed $3/2^-$ g.s. of ^{11}O is consistent with the recent Gamow coupled-channel calculations [75,77]. The g.s. of ^{10}Li is predicted to be a 2^+ state about 0.35 MeV above the neutron-emission threshold, in accordance with Ref. [63] while the lowest negative-parity state 1^- is expected to lie $\sim$1.0 MeV higher, in agreement with Ref. [71]. Due to a spectacularly strong Thomas-Ehrman effect, for ^{10}N we predict the 1^- g.s. and 2^- first excited state.

By successfully reproducing the structure of lithium isotopes and their mirror partners with an optimized interaction, we demonstrated that the quantified GSM is capable of quality predictions for exotic light nuclei with several valence protons and neutrons. Our future efforts will focus on Be and B isotopes, which exhibit complex structure due to the intricate effects of continuum coupling and clustering [83–87].

ACKNOWLEDGMENTS

Discussions with Kevin Fossez, Marek Płoszajczak, and Simin Wang are gratefully acknowledged as well as comments from Joshua Wylie. Computational resources were provided by the Institute for Cyber-Enabled Research at Michigan State University. This material is based upon work supported by the U.S. Department of Energy, Office of Science, Office of Nuclear Physics under Awards No. DE-SC0013365 (Michigan State University) and No. DE-SC0018083 (NUCLEI SciDAC-4 collaboration), and by the International Scientific Cooperation Conicet-NSF 1225-17.

[1] B. Jonson, Light dripline nuclei, Phys. Rep. **389**, 1 (2004).
[2] J. Al-Khalili and F. Nunes, Reaction models to probe the structure of light exotic nuclei, J. Phys. G **29**, R89 (2003).
[3] J. Dobaczewski, N. Michel, W. Nazarewicz, M. Płoszajczak, and J. Rotureau, Shell structure of exotic nuclei, Prog. Part. Nucl. Phys. **59**, 432 (2007).
[4] C. Forssén, G. Hagen, M. Hjorth-Jensen, W. Nazarewicz, and J. Rotureau, Living on the edge of stability, the limits of the nuclear landscape, Phys. Scr. **T152**, 014022 (2013).
[5] C. W. Johnson *et al.*, From bound states to the continuum, arXiv:1912.00451.
[6] N. Michel, W. Nazarewicz, J. Okołowicz, and M. Płoszajczak, Open problems in the theory of nuclear open quantum systems, J. Phys. G **37**, 064042 (2010).
[7] G. Hagen, T. Papenbrock, M. Hjorth-Jensen, and D. J. Dean, Coupled-cluster computations of atomic nuclei, Rep. Prog. Phys. **77**, 096302 (2014).
[8] G. Hagen, M. Hjorth-Jensen, G. R. Jansen, and T. Papenbrock, Emergent properties of nuclei from *ab initio* coupled-cluster calculations, Phys. Scr. **91**, 063006 (2016).
[9] P. Navrátil, S. Quaglioni, G. Hupin, C. Romero-Redondo, and A. Calci, Unified *ab initio* approaches to nuclear structure and reactions, Phys. Scr. **91**, 053002 (2016).
[10] S. Quaglioni, Light and unbound nuclei—An introduction to *ab initio* methods in nuclear structure and reaction theory, Eur. Phys. J. Plus **133**, 385 (2018).
[11] M. Freer, H. Horiuchi, Y. Kanada-En'yo, D. Lee, and U.-G. Meißner, Microscopic clustering in light nuclei, Rev. Mod. Phys. **90**, 035004 (2018).
[12] A. Calci, P. Navrátil, R. Roth, J. Dohet-Eraly, S. Quaglioni, and G. Hupin, Can *ab initio* Theory Explain the Phenomenon of Parity Inversion in ^{11}Be? Phys. Rev. Lett. **117**, 242501 (2016).
[13] A. Bonaccorso, F. Cappuzzello, D. Carbone, M. Cavallaro, G. Hupin, P. Navrátil, and S. Quaglioni, Application of an *ab initios* matrix to data analysis of transfer reactions to the continuum populating ^{11}Be, Phys. Rev. C **100**, 024617 (2019).
[14] S. Baroni, P. Navrátil, and S. Quaglioni, *Ab initio* Description of the Exotic Unbound ^{7}He Nucleus, Phys. Rev. Lett. **110**, 022505 (2013).
[15] S. Baroni, P. Navrátil, and S. Quaglioni, Unified *ab initio* approach to bound and unbound states: No-core shell model with continuum and its application to ^{7}He, Phys. Rev. C **87**, 034326 (2013).
[16] I. A. Mazur, A. M. Shirokov, A. I. Mazur, I. J. Shin, Y. Kim, P. Maris, and J. P. Vary, Description of continuum spectrum states of light nuclei in the shell model, Phys. Part. Nucl. **50**, 537 (2019).
[17] M. Vorabbi, A. Calci, P. Navrátil, M. K. G. Kruse, S. Quaglioni, and G. Hupin, Structure of the exotic ^{9}He nucleus from the no-core shell model with continuum, Phys. Rev. C **97**, 034314 (2018).
[18] A. Volya and V. Zelevinsky, Continuum shell model, Phys. Rev. C **74**, 064314 (2006).
[19] A. Volya and V. Zelevinsky, Continuum shell model and nuclear physics at the edge of stability, Phys. Atom. Nuclei **77**, 969 (2014).
[20] K. Bennaceur, F. Nowacki, J. Okołowicz, and M. Płoszajczak, A study of nuclei of astrophysical interest in the continuum shell model, J. Phys. G **24**, 1631 (1998).
[21] J. Okołowicz, M. Płoszajczak, and I. Rotter, Dynamics of quantum systems embedded in a continuum, Phys. Rep. **374**, 271 (2003).
[22] J. Rotureau, J. Okołowicz, and M. Płoszajczak, Theory of the two-proton radioactivity in the continuum shell model, Nucl. Phys. A **767**, 13 (2006).
[23] J. Okołowicz, M. Płoszajczak, and W. Nazarewicz, Convenient Location of a Near-Threshold Proton-Emitting Resonance in ^{11}B, Phys. Rev. Lett. **124**, 042502 (2020).
[24] N. Michel, W. Nazarewicz, M. Płoszajczak, and J. Okołowicz, Gamow shell model description of weakly bound nuclei and unbound nuclear states, Phys. Rev. C **67**, 054311 (2003).
[25] R. M. Id Betan, R. J. Liotta, N. Sandulescu, and T. Vertse, A shell model representation with antibound states, Phys. Lett. B **584**, 48 (2004).
[26] N. Michel, W. Nazarewicz, M. Płoszajczak, and T. Vertse, Shell model in the complex energy plane, J. Phys. G **36**, 013101 (2009).

[27] K. Fossez, J. Rotureau, N. Michel, and M. Płoszajczak, Can Tetraneutron Be a Narrow Resonance? Phys. Rev. Lett. **119**, 032501 (2017).

[28] N. Michel, J. G. Li, F. R. Xu, and W. Zuo, Description of proton-rich nuclei in the $A \approx 20$ region within the Gamow shell model, Phys. Rev. C **100**, 064303 (2019).

[29] A. Mercenne, N. Michel, and M. Płoszajczak, Gamow shell model description of ^{4}He(d, d) elastic scattering reactions, Phys. Rev. C **99**, 044606 (2019).

[30] M. D. Jones, K. Fossez, T. Baumann, P. A. DeYoung, J. E. Finck, N. Frank, A. N. Kuchera, N. Michel, W. Nazarewicz, J. Rotureau, J. K. Smith, S. L. Stephenson, K. Stiefel, M. Thoennessen, and R. G. T. Zegers, Search for excited states in ^{25}O, Phys. Rev. C **96**, 054322 (2017).

[31] Y. Jaganathen, R. M. Id Betan, N. Michel, W. Nazarewicz, and M. Płoszajczak, Quantified Gamow shell model interaction for *psd*-shell nuclei, Phys. Rev. C **96**, 054316 (2017).

[32] K. Fossez, J. Rotureau, and W. Nazarewicz, Energy spectrum of neutron-rich helium isotopes: Complex made simple, Phys. Rev. C **98**, 061302(R) (2018).

[33] http://www.nndc.bnl.gov/ensdf (2015).

[34] Y. Suzuki and K. Ikeda, Cluster-orbital shell model and its application to the He isotopes, Phys. Rev. C **38**, 410 (1988).

[35] T. Berggren, On the use of resonant states in eigenfunction expansions of scattering and reaction amplitudes, Nucl. Phys. A **109**, 265 (1968).

[36] L. Brillouin, *La méthode du champ self-consistent*, Exposés sur la théorie des quanta pub. some la direction de m. Léon Brillouin ... III; Actualités scientifiques et industrielles, Vol. 71 (Paris, Hermann & cie, 1933).

[37] I. Jae Shin, Y. Kim, P. Maris, J. P. Vary, C. Forssén, J. Rotureau, and N. Michel, *Ab initio* no-core solutions for ^{6}Li, J. Phys. G **44**, 075103 (2017).

[38] G. L. G. Sleijpen and H. A. Van der Vorst, A Jacobi-Davidson iteration method for linear eigenvalue problems, SIAM J. Matrix Anal. Appl. **17**, 401 (1996).

[39] J. Rotureau, N. Michel, W. Nazarewicz, M. Płoszajczak, and J. Dukelsky, Density Matrix Renormalization Group Approach for Many-Body Open Quantum Systems, Phys. Rev. Lett. **97**, 110603 (2006).

[40] J. Rotureau, N. Michel, W. Nazarewicz, M. Płoszajczak, and J. Dukelsky, Density matrix renormalization group approach to two-fluid open many-fermion systems, Phys. Rev. C **79**, 014304 (2009).

[41] I. Sick, Precise root-mean-square radius of ^{4}He, Phys. Rev. C **77**, 041302(R) (2008).

[42] H. Furutani, H. Horiuchi, and R. Tamagaki, Structure of the second 0^+ state of ^{4}He, Prog. Theor. Phys. **60**, 307 (1978).

[43] H. Furutani, H. Horiuchi, and R. Tamagaki, Cluster-model study of the $T = 1$ states in $A = 4$ system, Prog. Theor. Phys. **62**, 981 (1979).

[44] K. Fossez, J. Rotureau, N. Michel, and W. Nazarewicz, Continuum effects in neutron-drip-line oxygen isotopes, Phys. Rev. C **96**, 024308 (2017).

[45] K. Fossez, J. Rotureau, N. Michel, Q. Liu, and W. Nazarewicz, Single-particle and collective motion in unbound deformed ^{39}Mg, Phys. Rev. C **94**, 054302 (2016).

[46] P. Ring and P. Schuck, *The Nuclear Many-Body Problem* (Springer Verlag, Berlin/Heidelberg, 1980).

[47] C. Ordóñez and U. van Kolck, Chiral lagrangians and nuclear forces, Phys. Lett. B **291**, 459 (1992).

[48] P. F. Bedaque and U. van Kolck, Effective field theory for few-nucleon systems, Annu. Rev. Nucl. Part. Sci. **52**, 339 (2002).

[49] P. F. Bedaque, H. W. Hammer, and U. van Kolck, Narrow resonances in effective field theory, Phys. Lett. B **569**, 159 (2003).

[50] I. Stetcu, J. Rotureau, B. R. Barrett, and U. van Kolck, Effective interactions for light nuclei: An effective (field theory) approach, J. Phys. G **37**, 064033 (2010).

[51] P. Capel, V. Durant, L. Huth, H.-W. Hammer, D. R. Phillips, and A. Schwenk, From *ab initio* structure predictions to reaction calculations via EFT, J. Phys.: Conf. Ser. **1023**, 012010 (2018).

[52] B. A. Brown and W. A. Richter, New "USD" Hamiltonians for the *sd* shell, Phys. Rev. C **74**, 034315 (2006).

[53] L. Huth, V. Durant, J. Simonis, and A. Schwenk, Shell-model interactions from chiral effective field theory, Phys. Rev. C **98**, 044301 (2018).

[54] A. P. Zuker, Three-Body Monopole Corrections to Realistic Interactions, Phys. Rev. Lett. **90**, 042502 (2003).

[55] S. R. Stroberg, H. Hergert, S. K. Bogner, and J. D. Holt, Nonempirical interactions for the nuclear shell model: An update, Annu. Rev. Nucl. Part. Sci. **69**, 307 (2019).

[56] G. Hagen, M. Hjorth-Jensen, and N. Michel, Gamow shell model and realistic nucleon-nucleon interactions, Phys. Rev. C **73**, 064307 (2006).

[57] N. Michel, W. Nazarewicz, and M. Płoszajczak, Isospin mixing and the continuum coupling in weakly bound nuclei, Phys. Rev. C **82**, 044315 (2010).

[58] R. T. Birge, The calculation of errors by the method of least squares, Phys. Rev. **40**, 207 (1932).

[59] J. Dobaczewski, W. Nazarewicz, and P.-G. Reinhard, Error estimates in theoretical models: A guide, J. Phys. G **41**, 074001 (2014).

[60] R. P. Feynman, Forces in molecules, Phys. Rev. **56**, 340 (1939).

[61] N. Michel, H. Aktulga, and Y. Jaganathen, Toward scalable many-body calculations for nuclear open quantum systems using the Gamow Shell Model, Comp. Phys. Comm. **247**, 106978 (2020).

[62] H. Bohlen, A. Blazevic, B. Gebauer, W. V. Oertzen, S. Thummerer, R. Kalpakchieva, S. Grimes, and T. Massey, Spectroscopy of exotic nuclei with multi-nucleon transfer reactions, Prog. Part. Nucl. Phys **42**, 17 (1999).

[63] J. Smith, T. Baumann, J. Brown, P. DeYoung, N. Frank, J. Hinnefeld, Z. Kohley, B. Luther, B. Marks, A. Spyrou, S. Stephenson, M. Thoennessen, and S. Williams, Selective population of unbound states in ^{10}Li, Nucl. Phys. A **940**, 235 (2015).

[64] D. R. Tilley, C. M. Cheves, J. L. Godwin, G. M. Hale, H. M. Hofmann, J. H. Kelley, C. G. Sheu, and H. R. Weller, Energy levels of light nuclei $A = 5, 6, 7$, Nucl. Phys. A **708**, 3 (2002).

[65] http://www.tunl.duke.edu/nucldata/ (2015).

[66] M. Zinser, F. Humbert, T. Nilsson, W. Schwab, T. Blaich, M. J. G. Borge, L. V. Chulkov, H. Eickhoff, T. W. Elze, H. Emling, B. Franzke, H. Freiesleben, H. Geissel, K. Grimm, D. Guillemaud-Mueller, P. G. Hansen, R. Holzmann, H. Irnich, B. Jonson, J. G. Keller, O. Klepper, H. Klingler, J. V. Kratz, R. Kulessa, D. Lambrecht, Y. Leifels, A. Magel, M. Mohar, A. C. Mueller, G. Münzenberg, F. Nickel, G. Nyman, A. Richter, K. Riisager, C. Scheidenberger, G. Schrieder, B. M. Sherrill, H. Simon, K. Stelzer, J. Stroth, O. Tengblad, W. Trautmann, E. Wajda, and E. Zude, Study of the Unstable Nucleus ^{10}Li

in Stripping Reactions of the Radioactive Projectiles ^{11}Be and ^{11}Li, Phys. Rev. Lett. **75**, 1719 (1995).

[67] M. Thoennessen, S. Yokoyama, A. Azhari, T. Baumann, J. A. Brown, A. Galonsky, P. G. Hansen, J. H. Kelley, R. A. Kryger, E. Ramakrishnan, and P. Thirolf, Population of ^{10}Li by fragmentation, Phys. Rev. C **59**, 111 (1999).

[68] H. Jeppesen, A. Moro, U. Bergmann, M. Borge, J. Cederkäll, L. Fraile, H. Fynbo, J. Gómez-Camacho, H. Johansson, B. Jonson, M. Meister, T. Nilsson, G. Nyman, M. Pantea, K. Riisager, A. Richter, G. Schrieder, T. Sieber, O. Tengblad, E. Tengborn, M. Turrión, and F. Wenander, Study of ^{10}Li via the ^{9}Li(^{2}H, p) reaction at REX-ISOLDE, Phys. Lett. B **642**, 449 (2006).

[69] H. Simon, M. Meister, T. Aumann, M. Borge, L. Chulkov, U. D. Pramanik, T. Elze, H. Emling, C. Forssén, H. Geissel, M. Hellström, B. Jonson, J. Kratz, R. Kulessa, Y. Leifels, K. Markenroth, G. Münzenberg, F. Nickel, T. Nilsson, G. Nyman, A. Richter, K. Riisager, C. Scheidenberger, G. Schrieder, O. Tengblad, and M. Zhukov, Systematic investigation of the dripline nuclei ^{11}Li and ^{14}Be and their unbound subsystems ^{10}Li and ^{13}Be, Nucl. Phys. A **791**, 267 (2007).

[70] I. J. Thompson and M. V. Zhukov, Effects of ^{10}Li virtual states on the structure of ^{11}Li, Phys. Rev. C **49**, 1904 (1994).

[71] M. Cavallaro, M. De Napoli, F. Cappuzzello, S. E. A. Orrigo, C. Agodi, M. Bondí, D. Carbone, A. Cunsolo, B. Davids, T. Davinson, A. Foti, N. Galinski, R. Kanungo, H. Lenske, C. Ruiz, and A. Sanetullaev, Investigation of the ^{10}Li Shell Inversion by Neutron Continuum Transfer Reaction, Phys. Rev. Lett. **118**, 012701 (2017).

[72] A. Moro, J. Casal, and M. Gómez-Ramos, Investigating the ^{10}Li continuum through ^{9}Li(d, p)^{10}Li reactions, Phys. Lett. B **793**, 13 (2019).

[73] F. Barranco, G. Potel, E. Vigezzi, and R. A. Broglia, ^{9}Li(d, p) reaction as a specific probe of ^{10}Li, the paradigm of parity-inverted nuclei around the $N = 6$ closed shell, Phys. Rev. C **101**, 031305(R) (2020).

[74] G. V. Rogachev, J. J. Kolata, A. S. Volya, F. D. Becchetti, Y. Chen, P. A. DeYoung, and J. Lupton, Spectroscopy of ^{9}C via resonance scattering of protons on ^{8}B, Phys. Rev. C **75**, 014603 (2007).

[75] T. B. Webb, S. M. Wang, K. W. Brown, R. J. Charity, J. M. Elson, J. Barney, G. Cerizza, Z. Chajecki, J. Estee, D. E. M. Hoff, S. A. Kuvin, W. G. Lynch, J. Manfredi, D. McNeel, P. Morfouace, W. Nazarewicz, C. D. Pruitt, C. Santamaria, J. Smith, L. G. Sobotka, S. Sweany, C. Y. Tsang, M. B. Tsang, A. H. Wuosmaa, Y. Zhang, and K. Zhu, First Observation of Unbound ^{11}O, the Mirror of the Halo Nucleus ^{11}Li, Phys. Rev. Lett. **122**, 122501 (2019).

[76] N. Michel, W. Nazarewicz, M. Płoszajczak, and J. Rotureau, Antibound states and halo formation in the Gamow shell model, Phys. Rev. C **74**, 054305 (2006).

[77] S. M. Wang, W. Nazarewicz, R. J. Charity, and L. G. Sobotka, Structure and decay of the extremely proton-rich nuclei ^{11,12}O, Phys. Rev. C **99**, 054302 (2019).

[78] R. Sherr and H. T. Fortune, Energies within the $A = 10$ isospin quintet, Phys. Rev. C **87**, 054333 (2013).

[79] H. T. Fortune, Relative population of 0^+ states in ^{10}He in various reactions, Phys. Rev. C **88**, 054623 (2013).

[80] J. Hooker, G. Rogachev, V. Goldberg, E. Koshchiy, B. Roeder, H. Jayatissa, C. Hunt, C. Magana, S. Upadhyayula, E. Uberseder, and A. Saastamoinen, Structure of ^{10}N in ^{9}C+p resonance scattering, Phys. Lett. B **769**, 62 (2017).

[81] J. B. Ehrman, On the displacement of corresponding energy levels of C^{13} and N^{13}, Phys. Rev. **81**, 412 (1951).

[82] R. G. Thomas, An analysis ofthe energy levels of the mirror nuclei, C^{13} and N^{13}, Phys. Rev. **88**, 1109 (1952).

[83] N. Pillet, N. Sandulescu, and P. Schuck, Generic strong coupling behavior of Cooper pairs on the surface of superfluid nuclei, Phys. Rev. C **76**, 024310 (2007).

[84] Y. Lashko, G. Filippov, and V. Vasilevsky, Microscopic three-cluster model of ^{10}Be, Nucl. Phys. A **958**, 78 (2017).

[85] V. D. Rocca and F. Iachello, Cluster shell model: I. Structure of ^{9}Be, ^{9}B, Nucl. Phys. A **973**, 1 (2018).

[86] E. Garrido, D. Fedorov, and A. Jensen, Above threshold s-wave resonances illustrated by the $1/2^+$ states in ^{9}Be and ^{9}B, Phys. Lett. B **684**, 132 (2010).

[87] R. Álvarez-Rodríguez, A. S. Jensen, E. Garrido, and D. V. Fedorov, Structure and three-body decay of ^{9}Be resonances, Phys. Rev. C **82**, 034001 (2010).